INVESTIGATING THE IMPACTS OF TREE ALLOMETRY ON LIDAR-BASED TREE ABOVEGROUND BIOMASS MODEL PERFORMANCE

A THESIS SUBMITTED TO THE GRADUATE DIVISION OF THE UNIVERSITY

OF HAWAIʻI AT MĀNOA IN PARTIAL FULFILLMENT

OF THE REQUIREMENTS FOR THE DEGREE OF

MASTER OF ARTS

IN

GEOGRAPHY

MAY 2015

By
Rong Fang

Thesis Committee:

Qi Chen, Chairperson
David W. Beilman
Creighton M. Litton

Acknowledgements

I would like to express my appreciation to those who supported me to conduct this study. I would like to thank Dr. Qi Chen, for helping me develop this topic and guiding me through this research. Most importantly, Dr. Qi Chen has been remarkably influential with my scientific and academic development. I would like to thank my committee members Dr. David Beilman and Dr. Creighton Litton for providing me with critical knowledge of carbon sequestration and ecosystem ecology. Dr. David Beilman and Dr. Creighton Litton made significant contributions to my thesis writing, directing me to present my study in a structured way. Finally, I would like to thank my parents, Yang Liu and Jie Fang, and my boyfriend, Fangli Zhang, for the endless love and support.

Abstract

Airborne light detection and ranging (LiDAR) canopy height metrics are strong parameters for tree aboveground biomass (AGB) estimates. Since allometric models, in which tree diameter at breast height (DBH) and height are inputs, provide field AGB estimates in the LiDAR-AGB modeling processes, tree allometry is expected to impact the LiDAR-AGB model performance. The first objective of this study is to investigate how the tree height-DBH model fit impacts the LiDAR-AGB model performance. The second objective is to test how choices of allometric models for field AGB estimates influence the LiDAR-AGB model performance. A field data and simulation combined approach was employed. The primary findings showed that decline in the height-DBH model fit led to reduction in the LiDAR-AGB model performance. The secondary findings suggested that the LiDAR-AGB models developed from field AGB estimates based on both tree height and DBH outperformed models developed from field AGB estimates only based DBH.

Table of Contents

List of Tables

List of Figures

Chapter 1 Introduction

Global scale carbon balance affects change in climate. Forests are large terrestrial carbon sinks, and large proportions of carbon are stocked in forests as biomass(Myneni et al., 2001; Pacala et al., 2001; Pan et al., 2011). Tree aboveground biomass (AGB) is the total amount of living aboveground organic matter present in trees, including leaves, twigs, branches, main bole and bark (Brown 1997). Estimates of forest AGB plays an important role in estimating carbon stocks. Destructive harvest of trees provides the most accurate AGB estimates, but this approach is time- and labor- intensive and unrealistic in most cases. Due to widely present tree allometric relationships among tree characteristics (AGB, stem diameter, tree height, crown size etc.), field biomass is typically estimated through the construction and use of allometric models, which are developed with destructive AGB measurements and tree structural variables. Tree DBH is considered the most important variable in estimating tree aboveground biomass. Therefore, DBH-based equations (e.g., AGB = $a_0 DBH^{a_1}$, where a_0 and a_1 are fitted coefficients) have been established for AGB estimates at global scales (Bartelink, 1996; Basuki et al., 2009; Jenkins et al., 2003; Nelson et al., 1999; Ter-Mikaelian and Korzukhin, 1997; Zianis and Seura, 2005).

However, even with the use of allometric models, it is infeasible to measure every individual tree at large spatial scale. Remote sensing instruments enable biomass estimates at large scale, overcoming the difficulties of ground sampling (Gibbs et al., 2007). Previous studies have demonstrated that LiDAR is a reliable method to estimate AGB, because LiDAR is able to accurately estimate stand's characteristics (basal area, canopy mean height, tree density, stem volume, crown diameter etc.) (Lefsky et al. 1999; Hyde, Nelson et al. 2007; Chen et al. 2012). These forest structural characteristics are typically highly correlated with AGB. Different LiDAR systems successfully estimated AGB at the stand level, including airborne waveform LiDAR (Lefsky, Cohen et al. 1999; Anderson, Martin et al. 2006; Hyde et al. 2006), airborne discrete-return LiDAR (Lim et al. 2003; Patenaude et al. 2004; Næsset and Gobakken 2008; Asner et al. 2009; Zhao et al. 2009), and airborne profiling LiDAR (Bruneau et al. 2001; Nelson et al. 2004).

Regression analysis between field AGB estimated with traditional allometric approaches and LiDAR canopy height indices is the most common way to develop the LiDAR-AGB models. There is considerable variation in the coefficient of determination (R^2), a common measure of the goodness of fit, of LiDAR-AGB models across regions. The reported R^2 can vary from 0.56 to 0.96 (Asner et al., 2012; Hall et al., 2005; Means et al., 1999, 1999; Drake et al., 2003; Patenaude et al., 2004). The variations of R^2 could be related to many different factors such as i) whether lidar is integrated with other remotely sensed data (Anderson et al., 2008; Koetz et al., 2007; Lefsky et al., 2005; Swatantran et al., 2011), ii) statistical modeling approaches (Chen et al., 2010; Dalponte et al., 2008; Garcıa-Gutiérreza et al.; Gleason and Im, 2012),iii) lidar sensor types (Zolkos et al., 2013), iv) field plot size (Asner et al., 2012; Mascaro et al., 2011; Zolkos et al., 2013), and v) forest types (Zolkos et al., 2013; Nelson et al., 2007; van Leeuwen et al., 2011). Since AGB has been estimated via allometric methods with individual tree measurements (e.g., DBH and height) as inputs, it is expected that allometric methods will have large impacts LiDAR-based AGB model prediction. However, surprisingly, few studies have studied the impacts of allometric methods on LiDAR-based AGB model R^2 (Clark and Kellner, 2012; Zhao et al., 2012). Better understanding of sources causing variation in the LiDAR-AGB model performance is important to add knowledge of underlying mechanisms that hinder improvements of the LiDAR-AGB model performance, and plays an important role in error analysis of LiDAR-based AGB estimates.

R^2 is calculated as [1][1], where y_i is the observed value, $\bar{y}$ is the mean of the observed value, and $\hat{y}_i$ is the estimated value from regression model. For a given group of samples, y_i and $\bar{y}$ are observed values, thus R^2 is primarily determined by the sum of squared residuals (SSR). Large values of SSR will lead to small value of R^2. Using DBH-based AGB allometric models to estimate field AGB (see, e.g., Fig. 1.1b) will likely lead to large values of SSR in LiDAR-based AGB models (see Fig. 1.1c) as a result of variations in tree height at a given DBH (Fig. 1.1a), which in turn are reflected in the residuals — observed minus model predicted value — of tree height-DBH regression model. Because LiDAR measurements are mainly related to canopy vertical profile, variations in AGB at given tree height are hard to be detected by LiDAR. Thus, tree height-DBH model residuals are expected to impact the accuracy of the LiDAR-AGB model estimates.

Exactly how and to what extent tree level height-DBH allometric model residuals impact the plot level LiDAR-AGB models remain poorly understood. Large variance of height-DBH model residuals would challenge LiDAR's ability of estimating field AGB, because it increases the difficulty of canopy vertical variables to associate with DBH-based AGB estimates. Adding tree height in field AGB estimates is supposed to reduce the impacts of height-DBH model residuals on LiDAR model performance, due to including AGB variation at given tree height. Incorporating both DBH and height as inputs in field AGB estimates directly enhances the association between field AGB estimates and LiDAR canopy metrics (Zhao et al., 2012).

The objective of this study was to address two primary questions: 1) how do the height-DBH model residuals impact the goodness of fit of the LiDAR-AGB models? And 2) how does using different allometric models for field AGB estimates influence the LiDAR-AGB model

[1] $R^2 = 1 - \frac{\sum_{i=1}^{n}(y_i - \hat{y}_i)^2}{\sum_{i=1}^{n}(y_i - \bar{y})^2}$,

performance? To explore answers of these issues, a case study was conducted in a temperate conifer forest in Sierra Nevada, California. Two different allometric model systems were applied to generate field AGB estimates for developing the LiDAR-AGB models. A simulation approach was applied to test the impacts of the height-DBH model residuals on the LiDAR-AGB model performance.

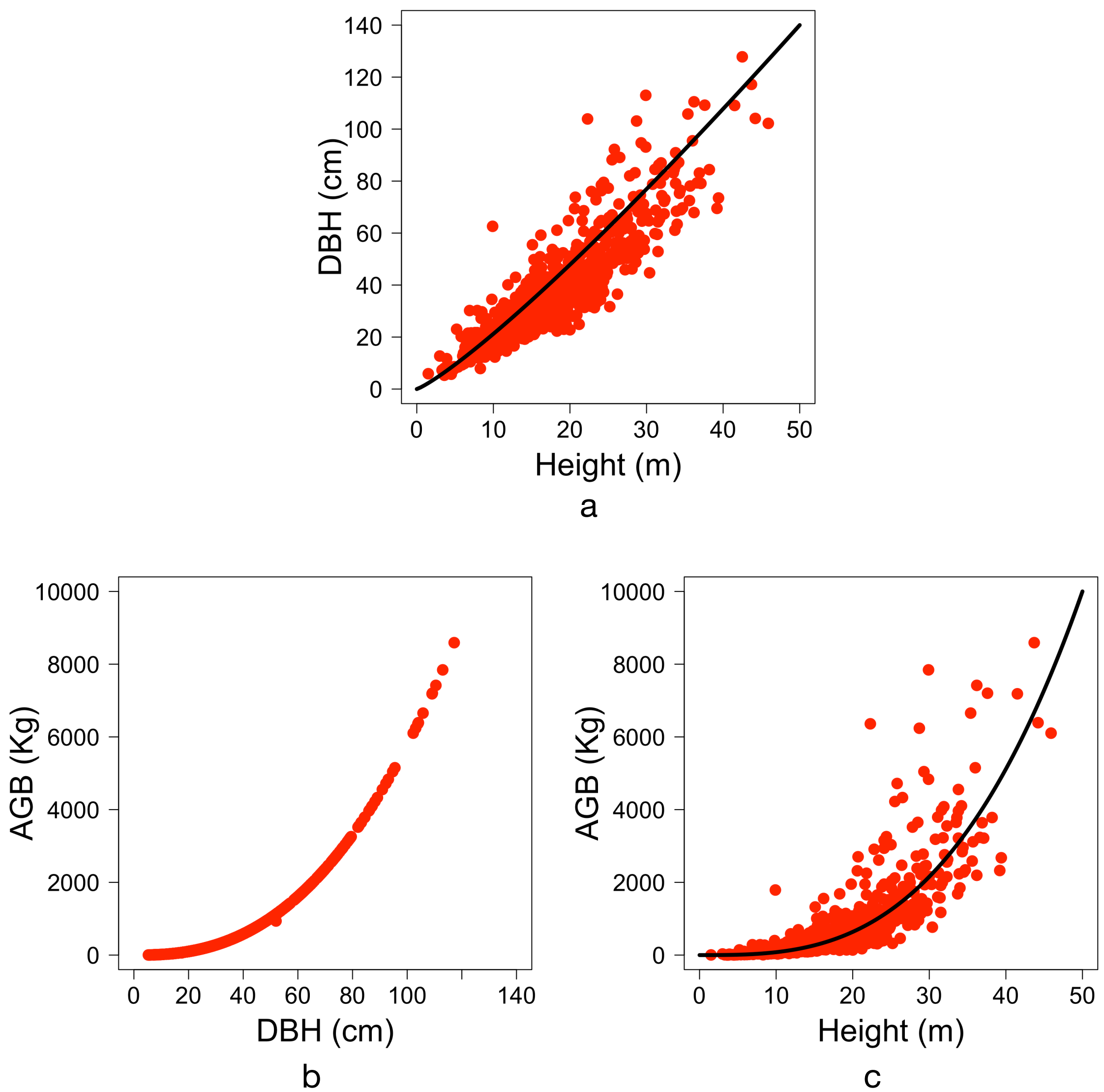

Figure 1.1 a: DBH vs. height; b: DBH-based tree aboveground biomass estimation model; c: tree height vs. tree aboveground biomass.

Chapter 2 Study area and data

2.1 Study site

This study site is located in the United States Forest Service Sagehen Creek Experimental Forest in California, which covers approximately 3925 ha and is on the eastern slope of the Sierra Nevada approximately 32 km north of Lake Tahoe (**Fig 2.1**). Conifer species present at this study site include white fir (*Abies concolor*), red fir (*Abies magnifica*), mountain hemlock (*Tsuga mertensiana*), lodgepole pine (*Pinus contorta*), Jeffrey pine (*Pinus jeffreyi*), aspen (*Populus tremuloides*), and western whitepine (*Pinus monticola*) (**Table 2.1**). Non-forested areas include fens, wet and dry montane meadows, and shrub fields. Elevation ranges from1862 m to 2670 m with slopes averaging 18% but can reach 70% in parts of the watershed (Chen et al., 2012).

Table 2.1 Major species present in this study area.

Species	Common name	Species code
Abies concolor	White fir	ABCO
Abies magnifica	California red fir	ABMA
Tsuga mertensiana	Mountain hemlock	TSME
Pinus contorta	Lodgepole pine	PICO
Pinus jeffreyi	Jeffrey pine	PIJE
Populus tremuloides	Aspen	PILA
Pinus monticola	Western whitepine	PIMO

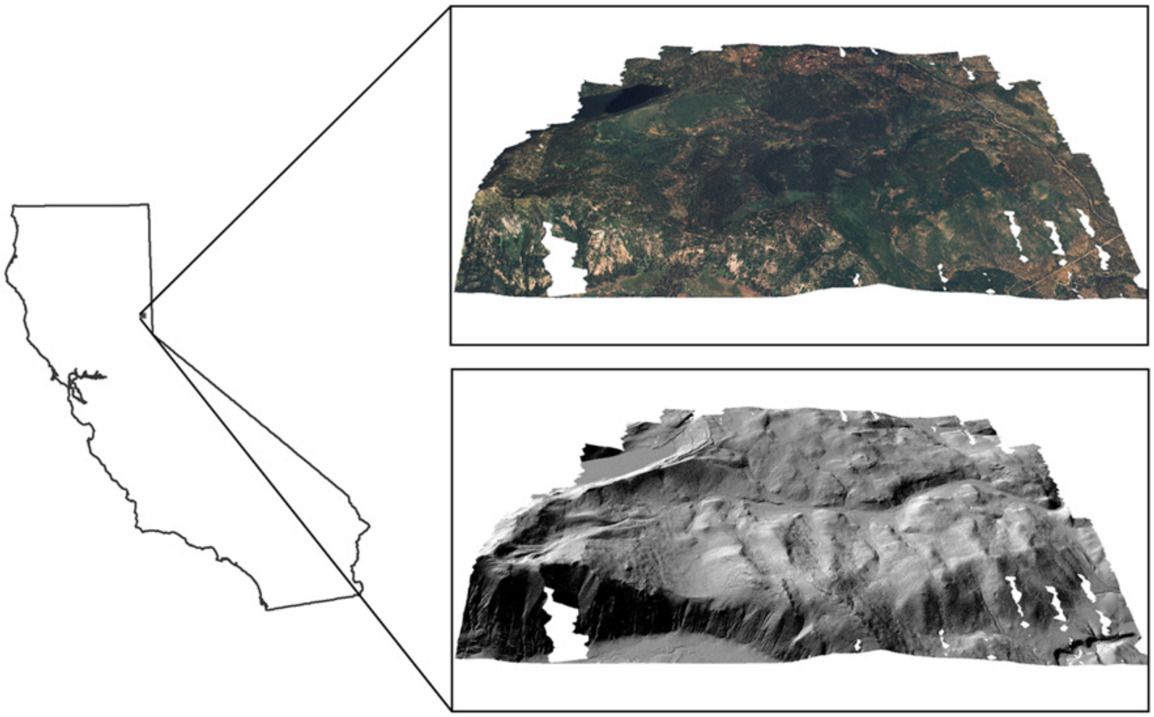

Figure 2.1 Location of the study area. Top-right: Aerial photographs draped over the LiDAR DEM. Bottom-right: A hillshade of the LiDAR DEM (Chen et al., 2012).

2.2 Data

2.2.1 Field data

A systematic sampling grid with sampling density 125 m was established (**Fig 2.2**). The locations of sampling plots were finally determined by a handheld Garmin eTrex recreational GPS with horizontal accuracy of 3 to 11 m for field sampling. Total 79 plots with both a recreational GPS and a differential GPS geo-reference were finally selected to construct the LiDAR-AGB models. The area of each circular sampling plot is 0.05 ha. All the field measurements were conducted by Chen et al., (2012) between 2004 and 2005.

At each plot, all trees greater than 5 cm in DBH were measured with a nested sampling design. Tree species, DBH, tree height, crown class crown ratio and vigor are measured. Vigor was defined into six different classes: 1) healthy trees with no visible defects, 2) healthy trees with minimal damage or defect (broken top/dead top, abnormal lean, etc.), 3) live trees that are near death or will be dead in the next five years, 4) recently dead trees with little decay and that retain their bark, branches and top, 5) trees that show some decay and have lost some bark, branches and may have a broken top, and 6) extensive decay and missing bark and most branches and have a broken top. The first three vigor classes are for live trees and the last three are for dead trees.

A total of 1393 trees, identified as dominant, co-dominant and intermediate crown classes, are finally used to develop the LiDAR-AGB models. These trees compose the overstory canopy, which are easily measured by LiDAR signals. Dead trees and suppressed trees are excluded from the LiDAR-AGB model constructions.

2.2.2 LiDAR data

LiDAR data were collected from September 14 to 17, 2005 for the study area using an

Optech ALTM 2050 system on an airplane flyingat an altitude of ~800 m and average velocity of 260 km per hour. The ALTM 2050 acquired up to three returns per pulse at a pulse frequencyof 50 kHz, scan frequency of 38 Hz, and a maximum scanangle of 15°, creating a swath width of ~580 m. The point density is about 2–4 returns per square meter. Optech, Inc. rates the RMSE precision of individual point locations surveyed by the ALTM 2050 as ±15 cm vertical and ±50 cm horizontal (Chen et al., 2012).

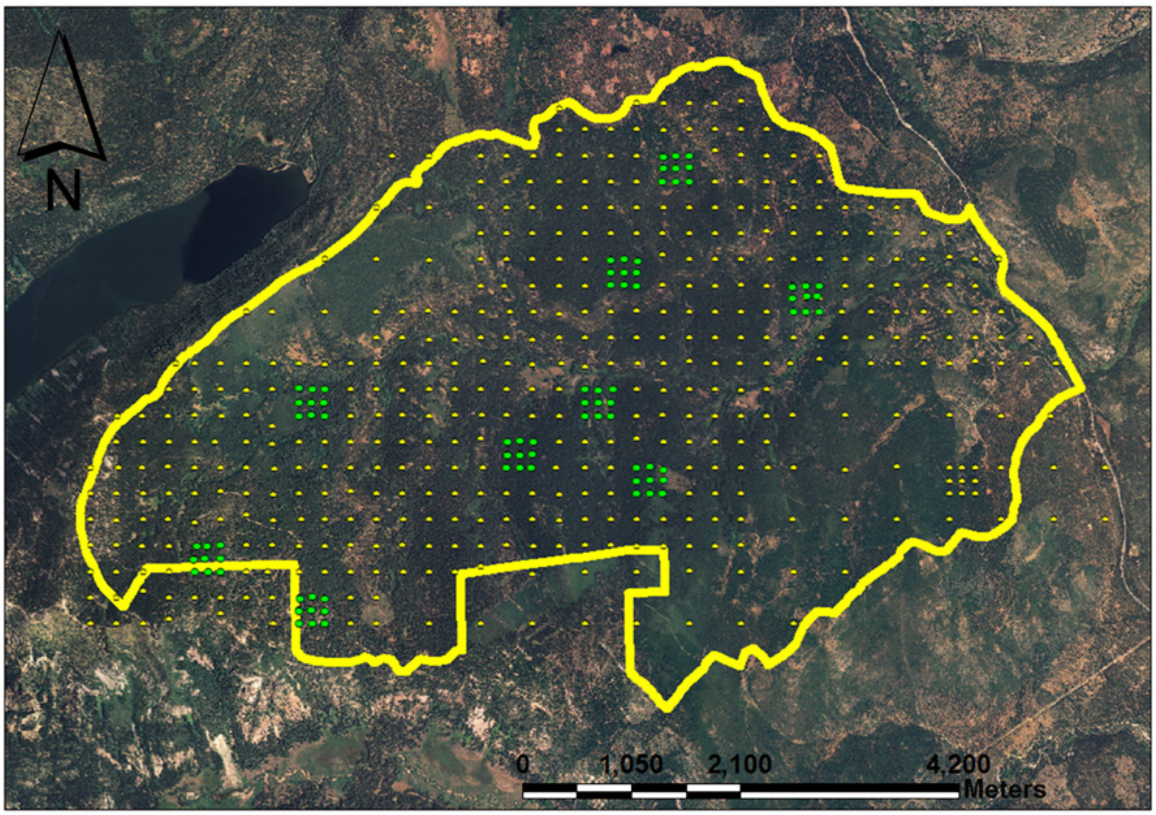

Figure 2.2 Field plots of vegetation measurements. The smaller dots indicate the plots located with a recreational GPS. The larger dots indicate the plots located with both a recreational GPS and a differential GPS. The thick line is the boundary of the vegetation (Chen et al., 2012).

Chapter 3 Methods

When the height-DBH model is perfectly fitted, LiDAR canopy height indices are expected to perform best in explaining variations of field AGB. In reality, residuals exist in the height-DBH model; thus, LiDAR's ability of predicting field AGB estimates is limited. Tree level height-DBH model and the plot level LiDAR-AGB models were constructed with simple linear regression processes at log-transformed scale. Root mean square residual (RMSR) was used to aggregate tree level height-DBH model residuals to plot level residual measure. Relationships between RMSR of the height-DBH model and absolute residuals of the LiDAR-AGB models were examined. Positive relationships between them indicate that the height-DBH model residuals are associated with errors of the LiDAR-AGB models. Furthermore, a simulation approach was employed to reveal the general pattern that how the height-DBH model residuals influence the LiDAR-AGB model performance.

Two sets of LiDAR-AGB models were compared: models constructed from field AGB estimates merely based on DBH, and models constructed from field AGB estimates based on both DBH and height. I used two AGB allometric model systems to derive field AGB estimates: Jenkins methods (Jenkins et al., 2003) and component ratio methods (CRM) (Heath et al., 2008). The former is a DBH-based AGB allometric model system, which was developed for national-wide tree AGB estimates. The latter is consistent with Jenkins AGB allometric system in definition of tree components (bark, bole, branch, and foliage), and it also includes species- and site-specific volume calibration and species specific gravity in the biomass calculation.

3.1 Field biomass calculation

In this study, only woody tree biomass was considered, including tree trunk, bark, branches and stump. Foliage biomass was excluded from calculations. First, individual tree AGB was calculated. Then, plot level AGB density (Mg/ha) was the summation of individual tree biomass in that plot divided by the plot area**:**

$$\mathrm{AGB_{plot}} = \frac{\sum_{i=1}^{n} \mathrm{AGB_i}}{\mathrm{Area_{plot}}} \qquad \textbf{Eq 3.1}$$

Where AGB_{plot} is the plot level aboveground biomass density (Mg/ha), AGB_i is the aboveground biomass of *ith* tree in the plot, n is the number of trees in the plot, and $Area_{plot}$ is the area of the plot.

3.1.1 Jenkins equation system

General form of Jenkins AGB allometric models are described as**:**

$$\mathrm{AGB} = e^{\beta_0+\beta_1 \ln(\mathrm{dbh})} \qquad \textbf{Eq 3.2}$$

where AGB is the tree total aboveground biomass, e is the base of the natural logarithm, β_0 and β_1 are parameters that are dependent on specific tree species group, DBH is diameter at breast height, and ln is natural logarithm.

Woody AGB is calculated as total AGB minus foliage AGB. Tree bole, branches and stump are different wood components. Tree component ratio is calculated as follows:

$$\mathrm{ratio} = e^{\beta'_0+\frac{\beta'_1}{\mathrm{DBH}}} \qquad \textbf{Eq 3.3}$$

where ratio is the ratio of a component to total aboveground biomass for trees, DBH is diameter breast height, e is the base of the natural logarithm, β'_0 and β'_1 are model coefficients that are determined by specific tree components.

Woody AGB is calculated as follows:

$AGB_{woody} = AGB * (1 - ratio_{foliage})$

where AGB_{woody} is the woody AGB, and $ratio_{foliage}$ is the foliage ratio.

Table 3.1 Parameter s for Jenkins aboveground biomass estimations.

Species code	Parameter	
	β_0	β_1
ABCO, ABMA,TSME	-2.5384	2.4814
PICO, PIJE, PIMO	-2.5356	2.4349
POTR	-2.2094	2.3867

Table 3.2 Parameters and equation for estimating foliage ratios of total aboveground biomass for hardwood and softwood species.

Species code	Biomass component	Parameter	
		β'_0	β'_1
Hard wood (POTR)	Foliage	–4.0813	5.8816
Softwood (ABCO,ABMA,PICO PIJE,PIMO)	Foliage	-2.9584	4.4766

3.1.2 Component ratio methods

Component ratio methods require the use of FIADB defined tree volume for the Pacific Northwest (Zhou and Hemstrom, 2010) and tree component ratios from Jenkins. The calculation process of CRM is as follow:

For trees > 5 inches DBH,

$AGB = DryBio_{bole} + DryBio_{stump} + DryBio_{top}$ **Eq 3.4**

where AGB is tree aboveground biomass, $DryBio_{bole}$ is the dry biomass from tree bole including wood and bark of the main stem of tree that also defines sound volume, $DryBio_{stump}$ is tree aboveground biomass from ground level to 1 foot stump, and $DryBio_{top}$ is the biomass from top and branches of the tree.

For trees < 5 inches DBH,

$\mathrm{DryBio}_{\mathrm{sapling}}$= ($\mathrm{BioSap}_{\mathrm{Jenkins}}$ – Foliage)* (1-Jenkins_Sapling_Adjustment) **Eq 3.5**

Where $\mathrm{DryBio}_{\mathrm{sapling}}$is the aboveground biomass of the sapling tree, $\mathrm{BioSap}_{\mathrm{Jenkins}}$is the aboveground biomass calculated using Jenkins model, Foliage is Jenkins et al. 2003 defined foliage biomass, and Jenkins_Sapling_Adjustment is the factor that adjusts Jenkins biomass for trees < 5 inches DBH (Heath et al., 2008). Table 3.4 and Table 3.5 are the FIA defined regional tree bole volume calculations and wood specific gravities for the species in this study, respectively.

$DryBio_{bole}$(Kg) = (VOLCFSND x 62.4 x SG_BARK x BRK_VOL_PROP) + (VOLCFSND x 62.4 X SG_WOOD) * 0.4536

where VOLCFSND is the volume of tree bole, BRK_VOL_PROP is Jenkins define bark ratio, SG_BARK is specific gravity of bark, SG_WOOD is the specific gravity of wood.

Top component ratio = (Jenkins total aboveground – Jenkins merchantable – Raile stump – Jenkins foliage) / (Jenkins merchantable)

where Raile stump (Kg) = DBH*DBH* RAILE_STUMP_B1 and Stump ratio = Raile stump/ Jenkins merchantable.

Thus, final tree aboveground biomass is defined as:

$$AGB = \text{DryBio}_{bole} + \text{DryBio}_{stump} + \text{DryBio}_{top}$$

$$= \text{DryBio}_{bole} * (1 + \text{Top component ratio} + \text{Stump component ratio}).$$

Table 3.3 FIA tree bole volume calculations for seven involved species (Zhou and Hemstrom, 2010).

Species	Equations
ABCO, ABMA	$e^{(-6.7013+1.7022*lnDBH+1.2979*lnHT)}$
PICO	$10^{(-2.615591+1.847504*log_{10}DBH+1.085772*log_{10}HT)}$
PIJE, PIMO	$10^{(-2.729937+1.909478*log_{10}DBH+1.085681*log_{10}HT)}$
POTR	$10^{(-2.63536+1.946034*log_{10}DBH+1.024793*log_{10}HT)}$
TSME	$0.001106485 * DBH^{1.8140497} * HT^{1.2744923}$

Table 3.4 Specific gravity of bark and wood for seven involved species (Zhou and Hemstrom, 2010).

Species	Bark specific gravity	Wood specific gravity
ABCO	0.56	0.37
ABMA	0.44	0.36
PICO	0.38	0.38
PIJE	0.36	0.37
PIMO	0.47	0.36
POTR	0.5	0.35
TSME	0.5	0.42

3.2 LiDAR processing

First, LiDAR point cloud was filtered and separated into ground and non-ground returns (Chen et al., 2007). The ground return was used to develop a Digital Elevation Model (DEM) of 1m cell size. Canopy height was derived as the subtractions of DEM cell elevation from individual points' z values. Multiple LiDAR height metrics were calculated (Table 3.6).

Table 3.5 LiDAR metrics (Chen et al., 2012).

LiDAR metrics	Description
$HT_{mean}, HT_{kurt}, HT_{std}$	Mean, standard deviation, skewness, kurtosis of height ofLiDAR points
$p_{0to5}, p_{5to10}, \dots, p_{>50}$	Proportion of LiDAR points within height bins (0 to 5 m, 5 to10 m, …, , and>50 m)
$h_5, h_{10}, \dots, h_{>100}$	Percentile height of LiDAR points
HT_{QDMH}	Quadratic mean height of LiDAR points

3.3 Nonlinear statistical modeling

McMahon (1971) found the power model ($L \propto D^{\alpha}$) could represent the general size and shape growing relationships between length and diameter of an organism (McMahon, 1971). Many studies constructed DBH-height models with linear regression analysis by logarithmically transforming DBH and tree height (Bartelink, 1996; Niklas, 1995; O'Brien et al., 1995). The tree height-DBH model was constructed with tree height as the independent variable and DBH as the dependent variable. At the individual tree level, height-AGB models were constructed to investigate if tree height is a strong parameter for AGB estimates. If individual tree height is a strong parameter of AGB, LiDAR canopy vertical measurements are expected to be powerful in predicting plot AGB as well.

For developing the LiDAR-AGB models, LiDAR mean canopy height (MCH) and quadratic mean canopy height (QMCH) are selected as the independent variables, since they are found to be most powerful parameters to associate with field AGB estimates (Asner et al., 2012; Lefsky et al., 1999; Means et al., 1999). Previous study found LiDAR MCH and QMCH were nonlinearly correlated to allometrically derived AGB estimates (Asner et al., 2012). Thus, the LiDAR-AGB models were also developed with simple linear regression at log-transformed scale.

Additionally, since DBH is the major variable correlated with tree age, I also constructed DBH-height models, in which DBH was the predictor and tree height was response variable. DBH-height model would be used to generate tree height for forest stands simulation.

All the nonlinear models were constructed with linear regression between logarithmically transformed explanatory and response variables as follows:

$$\ln(Y) = \alpha_0 + \alpha_1 * \ln(X) + e_0 \quad e_0 \sim N(O, \delta^2) \qquad \textbf{Eq 3.6}$$

where Y is the response variable, and X is the explanatory variables, α_0 and α_1 are the estimated parameters, and e_0 is the residual of the predictions.

Root mean square error (RMSE) and r^2 are two straightforward measures for the goodness of fit of linear models. The best model was evaluated with highest r^2 and lowest RMSE.

$$\mathrm{RMSE} = \sqrt[2]{\frac{\sum_{i=1}^{n}(\hat{y}_1 - y_i)^2}{n}} \qquad \textbf{Eq 3.7}$$

where $\hat{y_i}$ is the predicted value, y_i is the field AGB value, and n is the numbers of observations. Jenkins and CRM allometric models generate different AGB estimate. Thus, simply using RMSE to compare model performances is inappropriate. Instead of evaluating model performance with RMSE, I used relative RMSE to evaluate the model performance. Relative RMSE is given as RMSE/$\bar{y}$, where $\bar{y}$ is the mean of the field AGB values. Fitted models were further validated with leave-one-out validation. All the predicted values were back transformed and multiplied by a correction factor (CF) to address the issue of heteroscedastic variance of prediction errors (Baskerville, 1972) . The correction factor is s given by $\mathrm{CF} = e^{\mathrm{MSE}/2}$, where MSE isthe mean square error of the regression model.

3.4 The height-AGB model residuals vs. the height-DBH model residuals

Without tree height as an input, trees with same DBH are estimated to contain the same amount of AGB. Because there are large variations in tree height at given DBH, these variations cause residuals of height-AGB model. I expect the tree level height-DBH model would generate accumulative effect on height-based AGB estimates at plot level. I aggregated the tree level height-DBH and height-AGB model residuals to plot level residual measures by using root mean square residuals (RMSR), which are expressed as following:

$$\mathbf{RMSR_{DBH_i}} = \sqrt{\frac{\sum_{j=0}^{n}(\widehat{DBH}_j - \mathrm{DBH_j})^2}{n}} \qquad \textbf{Eq 3.8}$$

$$\mathrm{RMSR_{AGB_i}} = \sqrt{\frac{\sum_{j=0}^{n}(\widehat{AGB}_j - \mathrm{AGB_j})^2}{n}} \qquad \textbf{Eq 3.9}$$

where $\mathrm{RMSR_{DBH_i}}$ is the root mean square residual of DBH at plot i, $\widehat{\mathrm{DBH}}_\mathrm{j}$ is the estimated DBH of tree j in plot i from the height-DBH model, $\mathrm{DBH_j}$ is the field-measured DBH. $\mathrm{RMSR_{AGB_i}}$ is the root mean square residual of AGB of plot i, $\widehat{\mathrm{AGB}}_\mathrm{j}$ is the estimated AGB of tree j in plot i, and AGB_j is the field-estimated AGB from Jenkins and CRM allometric models.

Correlation between $\mathrm{RMSR_{DBH}}$ and $\mathrm{RMSR_{AGB}}$ reflects if height-DBH model residuals influence on plot-level height-based AGB estimates. Positive relationship between $\mathrm{RMSR_{DBH}}$ and $\mathrm{RMSR_{AGB}}$ indicates that height-DBH model residuals impact height-based AGB estimates. The greater the correlation denotes the larger impact of height-DBH model residuals on height-AGB model performance.

3.5 The LiDAR-AGB model residuals vs. the height-DBH model residuals

I further investigate impact of height-DBH model residuals on the LiDAR-AGB model. Accumulative height-DBH model residuals within a plot are supposed to cause residuals of LiDAR model. The absolute value of residuals of the LiDAR-AGB models are expressed as:

$$\mathrm{Resid_i} = |\widehat{\mathrm{AGB}}_\mathrm{i} - \mathrm{AGB_i}| \qquad \textbf{Eq 3.10}$$

where $\mathrm{Resid_i}$ is the absolute value of residual of LiDAR-AGB models constructed with Eq 3.6 for plot *i*. The correlation between $\mathrm{RMSR_{DBH}}$(Eq 3.8) and $\mathrm{Resid_i}$ reflects the impact of height-DBH allometry on performance of the LiDAR-AGB models. Positive correlation between them suggests that deviation of tree DBH from the fitted value of DBH-height model will lead to residuals of the LiDAR-AGB models.

3.6 Simulation

The increasing variance of residuals would lead to decrease the DBH-height model fit. I assume that the increasing variance of the DBH-height model residuals will cause reduction in the LiDAR-AGB model performance. Section 3.4 and section 3.4 only detect whether the height-DBH model residuals are correlated with residuals of the LiDAR-AGB models, however, these approaches do not test the hypothesis that increasing variances of residuals of logarithmically transformed DBH-height model would lead to decrease in R^2 of the LiDAR-AGB models. A simulation approach was applied to investigate how the log-transformed DBH-height model impacts LiDAR-AGB model performance.

Forest stands with different variances of the DBH-height model residuals were established (see Fig 3.1). Then, pseudo LiDAR point clouds were generated from the canopy surface. Finally, the LiDAR-AGB models were constructed from the AGB calibration of simulated stands and the canopy height indices derived from pseudo LiDAR point clouds. The simulation was coded with JAVA language under Eclipse Integrated Development Environment.

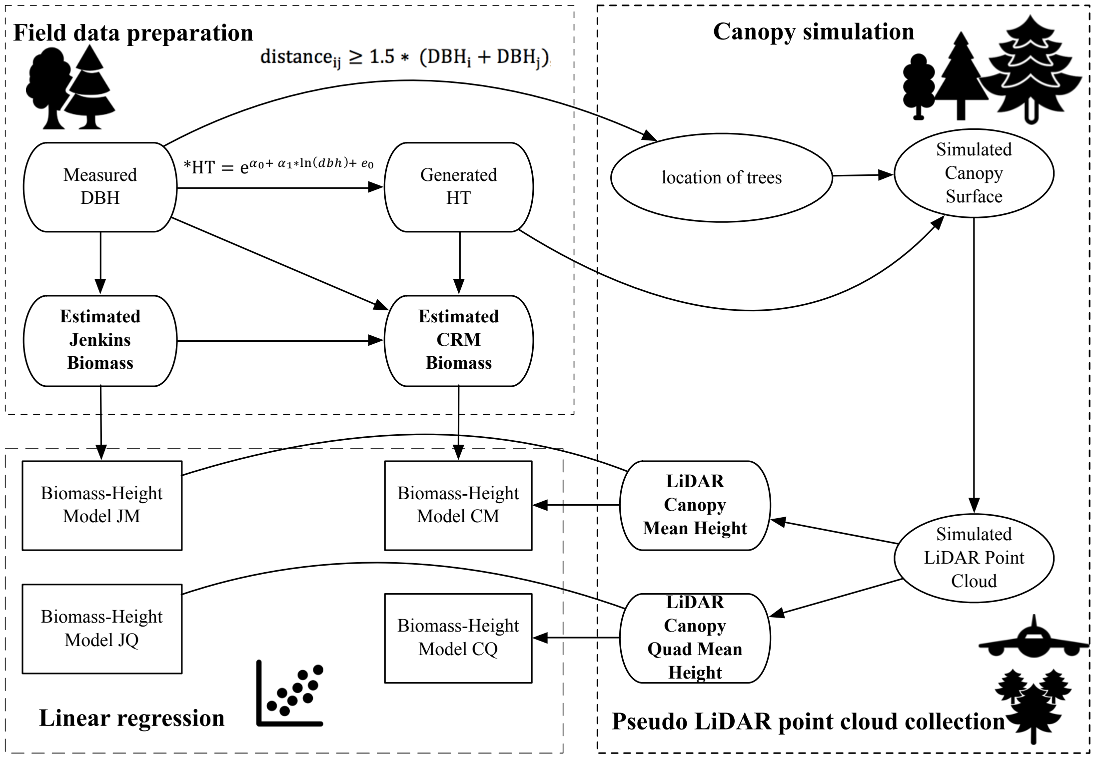

Figure 3.1 Forest stand and LiDAR point cloud simulation process. *refer the model general tree height from DBH, error term $\boldsymbol{e_0}$ is controlled as a random number from $\boldsymbol{N(0, R)}$, R is the variance of the normal distribution. The magnitude of R is controlled to simulate the dispersion of the error. R represents the general deviations of tree height from fitted value of the model.

Step 1: Deciding locations of trees

Simulated tree DBH and number of trees in a plot were determine by field measured Data. Since field tree location information was missing, for each plot, the first tree with was planted on a random location. Distance between any pairs of trees is determined with a rule that $\mathrm{distance}_{ij} \geq 1.5 * (\mathrm{DBH}_i + \mathrm{DBH}_j)$, where $\mathrm{distance}_{ij}$ is the distance between ith and jth trees in the same plot, DBH_i and DBH_j are the diameter at breast height of ith and jth trees; then, I move to next tree, till all trees' locations were determined (Fig 3.2).

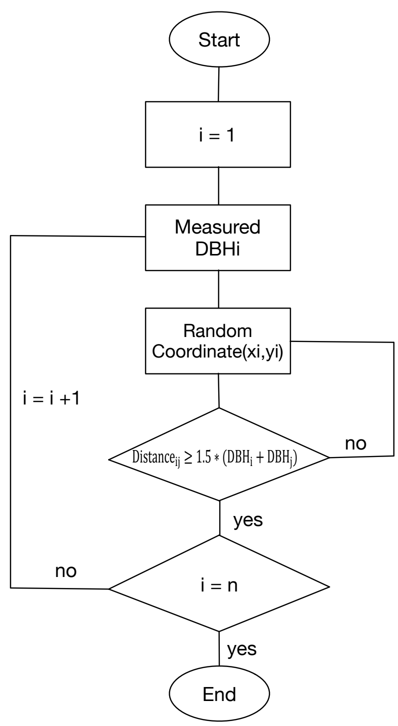

Figure 3.2 Process of setting locations for simulated trees.

Step 2: Estimating tree crown size and tree height

Crown size was determined by the crown positions. Crown sizes for dominant and co-dominant trees were determined with available models from Gill et al. (2001). Crown sizes for intermediate trees were determined with USDA Forest Vegetation Simulator described in Keyser and Dixon (2008). Tree crown was defined as symmetrical cone. Tree height was determined from the DBH-height model and plus a randomly generated error e_0 ($e_0 \sim N\ (0, \sigma^2)$). Crown ratio was obtained from field sampling. Total biomass of each plot was calculated with both Jenkins and CRM equations. The canopy surface was then derived from the established trees.

Step 3: Generate pseudo LiDAR point clouds

Pseudo LiDAR point clouds were collected from the simulated canopy surface with a density two to four returns per square meter. LiDAR MCH and QMCH were derived from the pseudo point clouds. All the returns were classified as ground returns and foliage returns. Thus, MCH and QMCH were calculated as:

$$MCH = \frac{\sum_{i=0}^{n} ht_i}{n} \qquad \textbf{Eq 3.12}$$

$$QMCH = \sqrt{\frac{\sum_{i=0}^{n} {ht_i}^2}{n}} \qquad \textbf{Eq 3.13}$$

where n is the total numbers of returns, ht_i is the height of *ith* element.

Step 4: Constructing LiDAR-AGB models

Field AGB estimates were calculated with Jenkins and CRM systems respectively. And Four LiDAR-AGB models were constructed by exhaustively combining of field AGB calibrations (Jenkins & CRM) and LiDAR metrics (MCH & QMCH).

Step 5: Changing the variance of the DBH-height model residuals

For each time, variance (σ_{e_0}) of the log-transformed DBH-height model residuals was increased by 0.05. Tree height was limited under 45 m, which was maximum tree height measured in this study area. Without controlling the upper limit of tree height, the increasing σ_{e_0} would not lead to change of slope and intercept of the log-transformed DBH-height model. However, the increasing σ_{e_0} finally generated extremely high value of tree height. The controlling upper limit of tree height will lead to downward (upward) change of slope (intercept) of log transformed height-DBH relationship. To eliminate effect of random locations of trees and canopy overlapping, 1000 realizations of simulated forest stands were created by repeating step 1 to 4, under each σ_{e_0} of the log-transformed DBH-height model.

Chapter 4 Results

4.1 Biomass calculations

As it shows in Table 4.1, without considering the height variation, Jenkins generated 23% higher mean plot woody AGB estimates than CRM. Plot estimated with most abundant aboveground biomass had AGB density 699 Mg/ha and 627 Mg/ha from Jenkins and CRM, respectively.

Table 4.1 Descriptive statistics for field AGB estimates.

Estimation Method	Total aboveground biomass Mg/ha			
	Mean	s.d.	Max	Min
Jenkins	223.46	147.99	699.30	19.04
CRM	181.81	123.54	626.56	12.19

4.2 Height-DBH models and height-AGB models

As it shows in the Fig 4.1 b and c, the height-Jenkins model generate larger variance of the residuals than the height-CRM model, and the greater variance is probably introduced by lack of AGB variation at given tree height.

At plot level, both $\mathrm{RMSR}_{\mathrm{AGB(Jenkins)}}$ and $\mathrm{RMSE}_{\mathrm{AGB(CRM)}}$ are significantly correlated with $\mathrm{RMSR}_{\mathrm{DBH}}$, implying the height-DBH model residuals influence accuracy of the height-AGB model estimates. The higher correlation between $\mathrm{RMSR}_{\mathrm{AGB}}$ and $\mathrm{RMSR}_{\mathrm{DBH}}$ suggests larger accumulative effect of the height-DBH model residuals on the height-AGB model performance. Expectedly, because of absence of tree height variation in AGB estimates, greater R^2 of 0.71 is found in $\mathrm{RMSR}_{\mathrm{AGB(Jenkins)}}$ vs. $\mathrm{RMSR}_{\mathrm{DBH}}$. In comparison, R^2 of $\mathrm{RMSR}_{\mathrm{AGB(CRM)}}$ vs. $\mathrm{RMSR}_{\mathrm{DBH}}$ is weaker with a value of 0.59, suggesting applying CRM in AGB estimates reduces the scatter of relationship between tree height and AGB. Since tree height and LiDAR metrics are canopy vertical structure, Therefore, the increasing association between tree height and CRM AGB estimates is expected to enhance LiDAR's ability of predicting field AGB estimates.

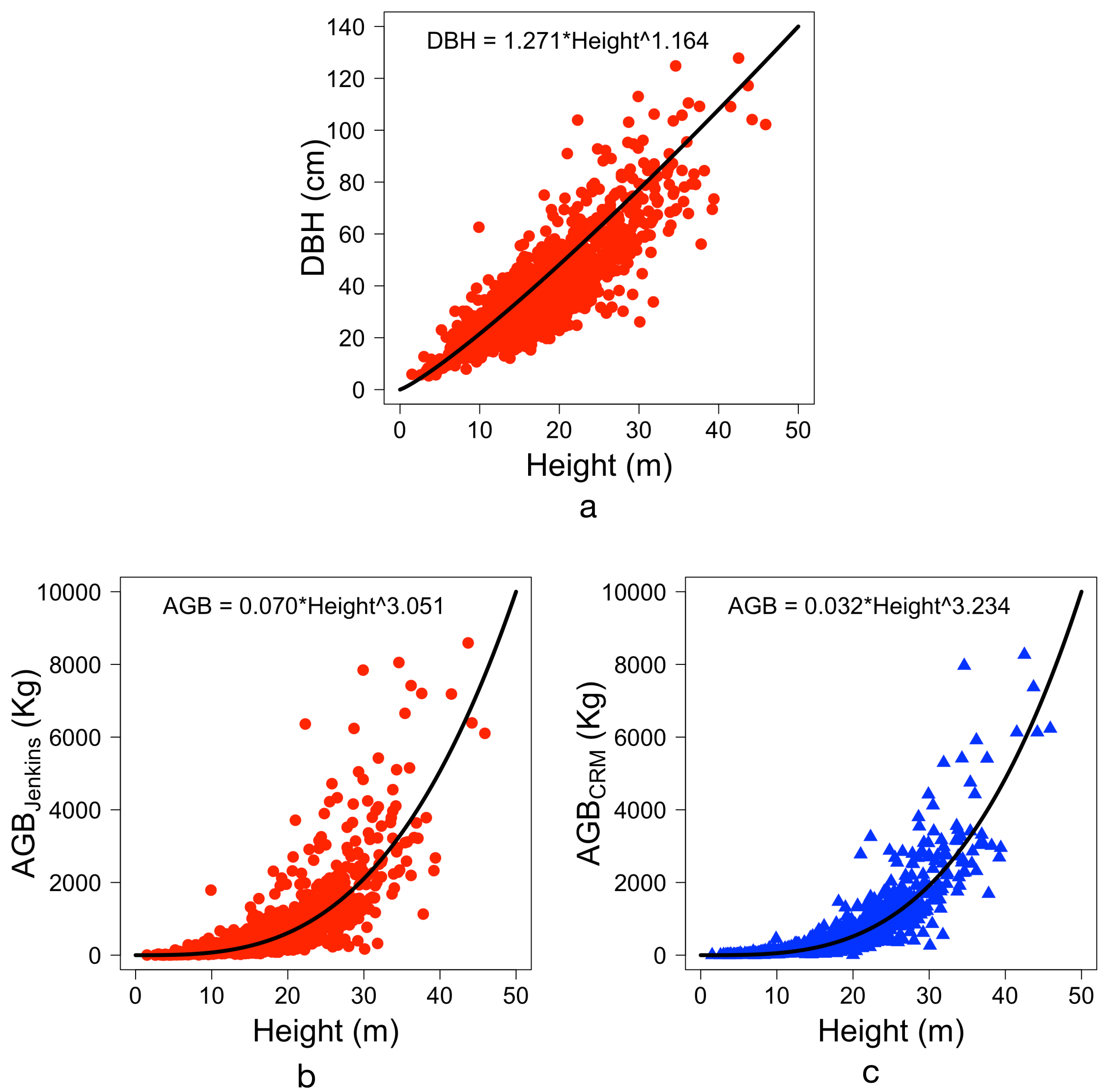

Figure 4.1 a: the DBH-height model; b: the Jenkins AGB-height model; c: the CRM AGB-height model.

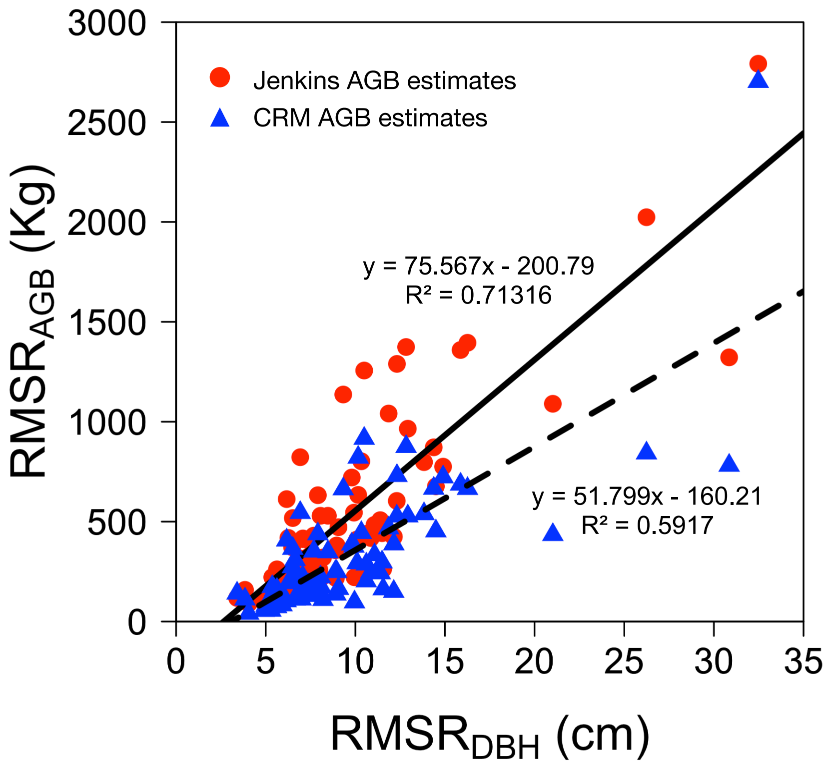

Figure 4.2 Relationships between root mean square residual of DBH-height models and AGB-height models. Upper: AGB model derived from Jenkins allometric models; lower: AGB model derived from CRM allometric models.

4.3 LiDAR-AGB models

Four LiDAR models were constructed (Table 4.2). The results show that QMCH is a better parameter of field AGB derived from both Jenkins and CRM allometric models. Model CQ outperformed model JQ, producing higher R^2 (0.82 vs. 0.76) and lower relative RMSE (0.29 vs. 0.37). As it shows in Fig 4.2, Although regression lines of observed vs. predicted for four models were not significantly different from the identical line (1:1), the variances of the model residuals were lower in model CQ (CM) than model JQ (JM).

Table 4.2 Coefficients LiDAR biomass estimation model ($lnAGB = a_0 + a_1 * \ln ht_{lidar}$).

Model	a_0	Standard Error	P-value	a_1	Standard Error	P-value	R^2	RMSE (Mg/ha)	Relative RMSE
JM	3.4900	0.1292	<2e-16	1.0429	0.0748	<2e-16	0.716	99.142	0.4437
CM	3.1518	0.1223	<2e-16	1.1238	0.0710	<2e-16	0.773	72.097	0.3929
JQ	1.7007	0.2236	5.8e-11	1.5665	0.0988	<2e-16	0.766	81.682	0.3655
CQ	1.2237	0.2048	5.4e-07	1.6883	0.0905	<2e-16	0.820	53.896	0.2937

Note: JM is model developed with LiDAR mean canopy height and Jenkins AGB estimation; CM is model developed with LiDAR mean canopy height and CRM AGB estimation; JQ is model developed with LiDAR quadratic mean canopy height and Jenkins AGB estimation; CQ is model developed with LiDAR quadratic mean canopy height and CRM AGB estimation.

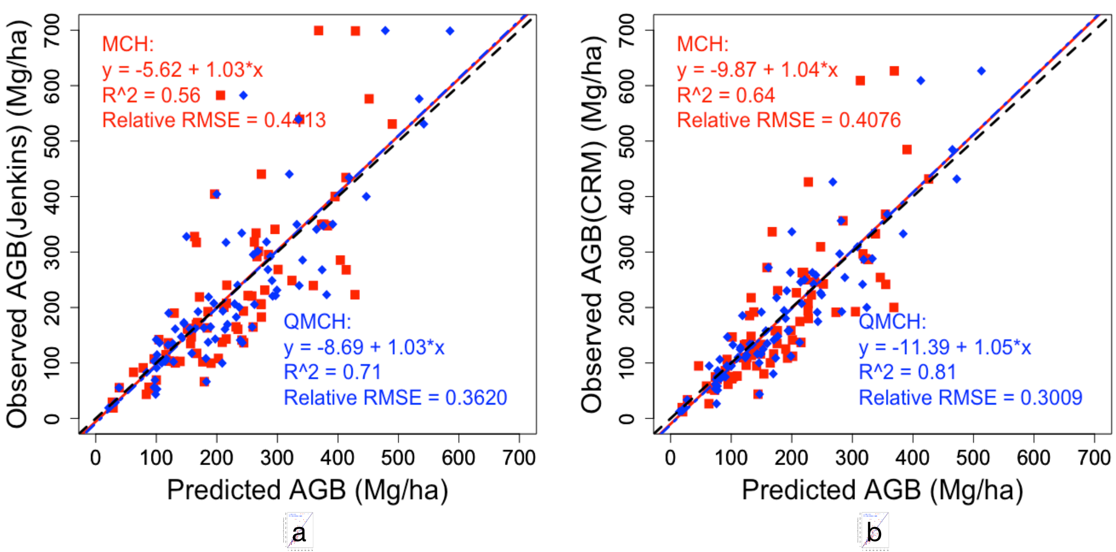

Figure 4.3 a: Jenkins field-measured AGB against LiDAR aboveground biomass estimates; **b:** CRM field-measured AGB against LiDAR aboveground biomass estimates; red square indicates aboveground biomass estimates of the LiDAR-MCH-based models, blue diamond indicates aboveground biomass estimates of LiDAR-QMCH-based models, dash line is 1:1 reference line.

Plot level $RMSE_{DBH}$ was significantly correlated with absolute value of the LiDAR-AGB model residuals. R^2 was stronger in AGB models derived from Jenkins AGB estimates (0.16 & 0.20) than AGB models derived from CRM AGB estimates (0.10 & 0.17) (**Fig 4.6**), suggesting that the height-DBH model residuals have larger impact LiDAR-AGB models derived from Jenkins AGB estimates. The correlations were also stronger in AGB models derived from QMCH. This is probably because more weights are given to each height elements, and the impact of the height-DBH model residuals was amplified.

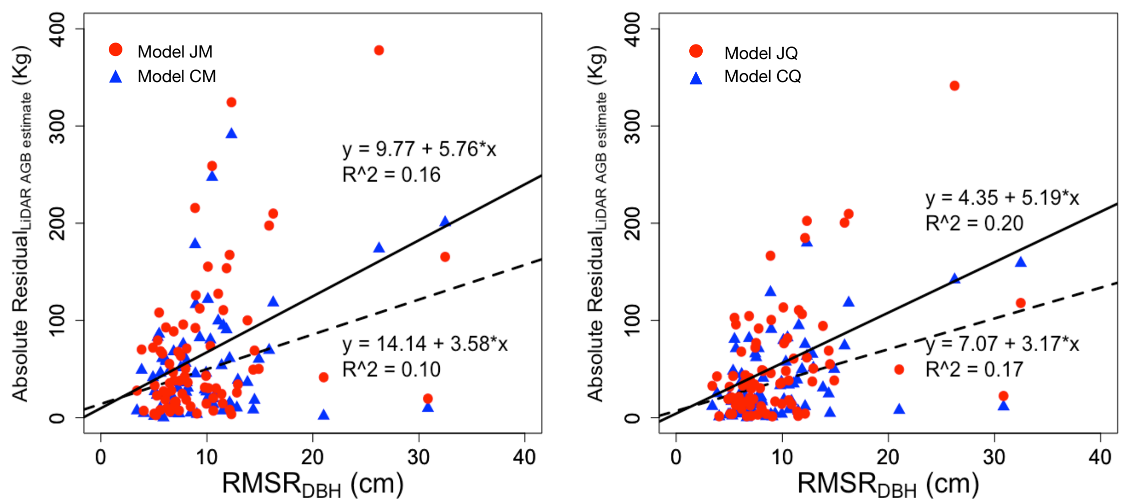

Figure 4.4 Absolute value of the LiDAR-AGB model residuals vs. root mean square height-DBH model residuals.

4.5 Simulation

4.5.1 Simulated plot establishment and AGB calculation

Plots with different variance of the log-transformed DBH-height model residuals were established (Fig 4.5). Increasing variance of the log-transformed DBH-height model residuals led to change in slope, intercept and R^2 of the fitted model (Fig 4.6). When σ_{e_0} from 0.05 to 0.5, mean R^2 decease from 0.98 to 0.28, the slope drop from 0.71 to 0.62, and the intercept increase from 0.3 to 0.60.

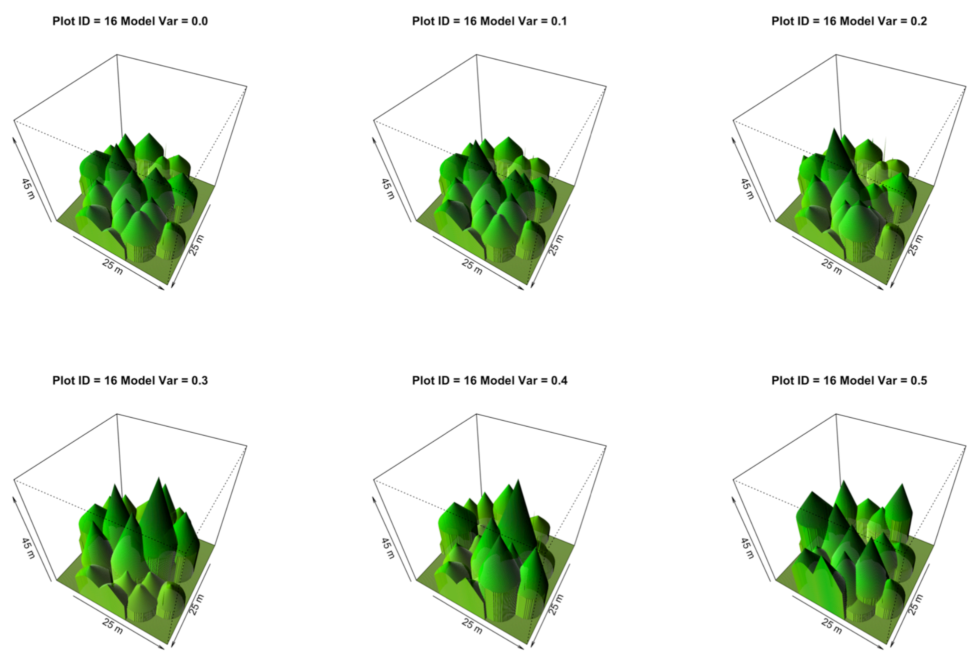

Figure 4.5 Simulated forest sampling plot with different variability of height-DBH relationship.

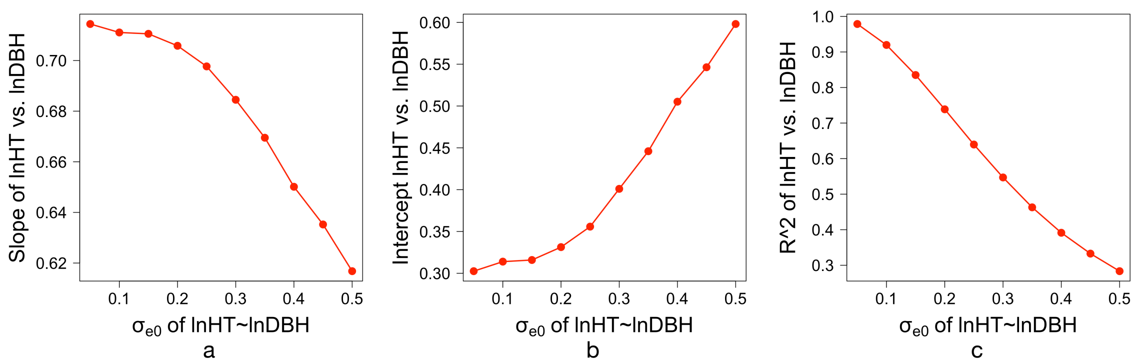

Figure 4.6 Trends of slopes, intercepts and $\boldsymbol{R^2}$of lnHT vs. lnDBH, as the $\boldsymbol{\sigma_{e_0}}$ increases. Each point indicates the mean of 1000 realizations.

4.5.2 Constructions of AGB models with pseudo LiDAR metrics

The model comparisons were conducted between models constructed with different field AGB estimates and different LiDAR canopy height indices. I mainly compared two aspects of models' sensitivities: 1) the goodness of fit and 2) stability of estimated slopes and intercepts.

As variance of the DBH-height model residuals increased from 0.05 to 0.5 at log-transformed scale, relative RMSE of model JQ increased from 23% to 45% (Fig 4.7 d). In contrast, relative RMSE of model CQ only increased from 23% to 29%. Similar pattern was found in comparison of model JM and CM. Relative RMSE of model JM increased from 36% to 48%, and relative RMSE of model CM kept constant around 34% (Fig 4.7 d). These patterns demonstrated that performance of LiDAR-AGB models constructed based on Jenkins AGB estimates was more sensitive to the decreasing DBH-height model fit. Furthermore, model CM also show strong stability that the slope and intercept of model CM were not strongly influenced by the changing slope and intercept of the log-transformed height-DBH model. Similar trends are also found in QMCH-based models. Thus, LiDAR-AGB models constructed based on CRM AGB estimates were not only robust in their model performance but also stable in the estimated parameters.

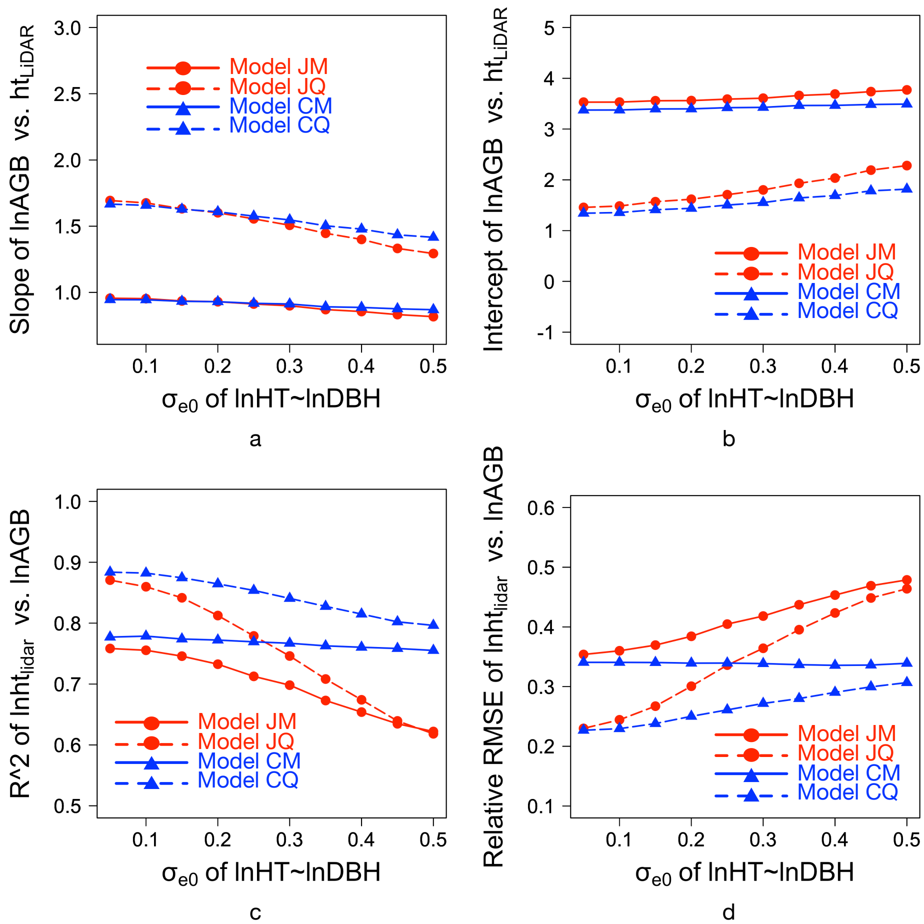

Figure 4.7 Trends of parameters of LiDAR-AGB models, as the $\boldsymbol{\sigma_{e_0}}$ of lnHT-lnDBH relationship increase, a: slope, b: intercept, c: $\boldsymbol{R^2}$ and d: relative RMSEs. Every point represents average of 1000 realizations at given $\boldsymbol{\sigma_{e_0}}$. Red solid line indicates model JM; red dashed line indicates model JQ; blue solid line indicates model CM, blue dashed line AGB model CQ.

Chapter 5 Discussion

This study aims at investigating the underlying mechanisms driving the variation in the LiDAR-AGB model performance. Previous studies have extensively examined the sources causing the change in the LiDAR model performance. Integration LiDAR data with optical imageries could improve the AGB estimate results (Anderson et al., 2008; Koetz et al., 2007; Lucas et al., 2008; Swatantran et al., 2011), because the latter could provide canopy biophysical, chemical and geometric properties, which are highly related to the tree productivity. Increasing plot size could reduce errors of LiDAR-based AGB estimates (Asner et al., 2012; Mascaro et al., 2011; Zolkos et al., 2013). Applications of machine learning approaches could also increase LiDAR performance in AGB estimates, because machine learning approaches take the internal correlations and underlying nonlinearity among canopy structural variables into account (Chen et al., 2010; Dalponte et al., 2008; Garcıa-Gutiérreza et al.; Gleason and Im, 2012).

Most studies focused on improving model performance by manipulating external data processing. However, few studies researched on the forest intrinsic structural factors that fundamentally constraint the LiDAR model performance. Although few studies mentioned that variations in tree height at similar DBH introduce errors to LiDAR-based AGB estimates (Clark and Kellner, 2012; Zolkos et al., 2013), none of these studies used quantitative method to assess variation of the LiDAR-AGB model performance caused by this forest stands' inherent property. This study improves the understandings of tree allometry's impacts on accuracy of LiDAR-based AGB estimates.

5.1 Impacts of tree allometry on LiDAR model performance

My objectives are to answers two questions: 1) how do the tree level height-DBH allometric model residuals impact the plot level LiDAR-AGB models? And 2) how does using different allometric models for field AGB estimates influence the LiDAR-AGB model performance? Truly measured data test and simulation results provided explanations for these questions. Truly measured data was important for manifesting the ground truth phenomenon. The simulation further confirmed truly measured data results, revealing the general pattern — how the LiDAR-AGB model performance vary with the change in the height-DBH model fit and how the model performance varies in models constructed from different field AGB estimates.

All the nonlinear models were developed with simple linear regression at log-transformed scale. Although log transformed linear modeling approach may not provide the best model fit results, the simplified model form could straightforwardly describe the height-DBH and the LiDAR-AGB relationships. Thus, it is plausible to compare two sets of model residuals at different spatial levels.

My primary results showed that plot level RMSR of the height-DBH model was correlated with absolute value of all LiDAR-AGB model residuals. It manifested that the tree level height-DBH model residuals generated accumulative effect on accuracy of plot level LiDAR-based AGB estimates. In a word, scatter of the height-DBH relationship limits LiDAR's ability of estimating AGB. But it has to be noticed that heteroscedastic variance of log transformed linear model residuals also contributed to strong correlations between the height-DBH and LiDAR-AGB model residuals. Moreover, these correlations varied in models developed based on different field AGB estimates, suggesting that the extent of the height-DBH allometry impact on LiDAR model performance depends on whether tree height is included in field AGB estimates. Zhao et al. (2012) found choices of allometric models impact the LiDAR-AGB model performance. In consistent with Zhao et al. (2012), my results showed LiDAR models developed from field AGB estimates based on both tree height and DBH outperformed models developed from field AGB estimates only based on DBH. If tree height is absent from field AGB estimates, LiDAR could generate misleading AGB estimates. I extended their work, not only comparing the LiDAR-AGB model performance, but also associating the difference in the LiDAR-AGB model performance with impacts from the height-DBH model residuals.

Simulation results further confirmed that the height-DBH model residuals would introduce errors to LiDAR-based AGB estimates. Increasing variance of the height-DBH model residuals led to the reduction in the LiDAR-AGB model performance, though the severity of the reduction trends differed in the LiDAR-AGB models developed from different field AGB estimates and LiDAR canopy metrics. The LiDAR-AGB model performance reductions were slower in models constructed from field AGB estimates based on both tree height and DBH remained relatively constant, as the variance of the log-transformed height-DBH model residuals increase.

Hence, applications of allometric models including tree height as an input in the LiDAR-AGB modeling processes not only improves LiDAR canopy metrics' ability of estimating AGB, but also enhances robustness of the LiDAR-AGB model performance towards to the increasing variance of the height-DBH model residuals. This finding also demonstrates that LiDAR is reliable in estimating canopy timber volume.

5.2 Potential of increasing LiDAR-based AGB model accuracy

When the height-DBH model was well fitted ($R^2 = 1$), there were considerable (>20%) errors in the LiDAR-AGB models. Since systematic or random errors did not exist in measurements of simulated data, these errors were attributed to canopy overlapping and the underlying nonlinearity between tree-level AGB and plot-level AGB. High accurate LiDAR-AGB model estimates are preferable. $\pm$10% relative RMSE is the standard. However, even errors introduced by tree allometry were excluded; the best LiDAR-AGB model only achieved 23% relative RMSE. Although using multiple LiDAR metrics, integrating LiDAR data with other remote sensing data and applications of advanced statistical modeling approaches could also largely improve the LiDAR-AGB model performance, these models, developed from one study site, are not applicable to other study sites. Considering the relative small plot size and LiDAR sampling density of this study, the LiDAR-AGB model performance could be further improved by increasing the plot size and point cloud density.

5.3 Tree height in estimates of AGB

Since field tree height measurements are less accessible than DBH, the necessity of including tree height in field sampling is concerned. Particularly, uncertainties of tree allometry increase with the forest structural complexity in primary forest, where there is need to sample tree height in field measurements. Many studies have successfully estimate individual tree height via LiDAR measurements, and the difficulties of LiDAR individual tree height measurements lie on tree crown and top identifications (Chen et al., 2006; Edson and Wing, 2011; Falkowski et al., 2006; Hyyppa et al., 2001; Kwak et al., 2007). Incorporating LiDAR individual tree height measurements and field DBH in developing the LiDAR-AGB models could potentially increase the model performance.

5.4 Limitations

Finally, there were limitations in the simulation approach. This simulation approach only considered the variation in DBH-height relationship. The variations of crown size and crown ratio were not taken into consideration. Crown sizes were estimated from exiting DBH-crown-size models. Crown ratio was collected from field sampling. They were fixed values at each simulation. Crown size estimation would determine the canopy cover rate of simulated sampling plots. Since LiDAR canopy height indices were extracted by weighing crown size, crown size estimation would also contribute the disparity between simulated and truly measured data.

Conclusion

This study was driven by investigating an underlying factor — the height-DBH model residuals — that fundamentally constraints the LiDAR-AGB model performance. Since allometric models provide field AGB estimates in LiDAR-AGB modeling processes, the scatter relationships among tree structural variables inevitably introduce errors to the LiDAR-AGB models. Without considering the internal relationships among tree structural variables, models developed from one site cannot be directly compared with models developed from other sites. Although previous studies stated tree allometry is not a major factor strongly influencing the LiDAR-AGB model performance, my primary findings suggested that decline in the height-DBH model fit led to apparent reduction in the LiDAR-AGB model performance. Especially, when inappropriate allometric models were selected in field AGB estimates, the LiDAR-AGB models were severely influenced by the height-DBH allometry. In this study, I compared two allometric model systems for field AGB estimates: Jenkins and CRM. The latter was found preferable in constructing the LiDAR-AGB models. First of all, models developed based on CRM field AGB estimates outperformed models developed based on Jenkins field AGB estimates in goodness of fit, generating less relative RMSE. Secondly, the performance of models developed based on CRM field AGB estimates remained robust with the increasing variance of the height-DBH model residuals.

Although field tree height measurements are difficult to achieve in closure canopy area, I recommend combining LiDAR individual tree height estimates with field DBH measurements to examine the relationship between height and DBH, when researchers develop the LiDAR-AGB models. Assessing variance of the height-DBH model residuals plays an important role in directing researchers to select appropriate allometric models for field AGB estimates, and it also sever as an guidance in error analysis of the LiDAR-based AGB estimates.

References

Anderson, J.E., Plourde, L.C., Martin, M.E., Braswell, B.H., Smith, M.-L., Dubayah, R.O., Hofton, M.A., and Blair, J.B. (2008). Integrating waveform lidar with hyperspectral imagery for inventory of a northern temperate forest. Remote Sens. Environ. *112*, 1856–1870.

Asner, G.P., Mascaro, J., Muller-Landau, H.C., Vieilledent, G., Vaudry, R., Rasamoelina, M., Hall, J.S., and van Breugel, M. (2012). A universal airborne LiDAR approach for tropical forest carbon mapping. Oecologia *168*, 1147–1160.

Bartelink, H.H. (1996). Allometric relationships on biomass and needle area of Douglas-fir. For. Ecol. Manag. *86*, 193–203.

Baskerville, G.L. (1972). Use of logarithmic regression in the estimation of plant biomass. Can. J. For. Res. *2*, 49–53.

Basuki, T.M., van Laake, P.E., Skidmore, A.K., and Hussin, Y.A. (2009). Allometric equations for estimating the above-ground biomass in tropical lowland Dipterocarp forests. For. Ecol. Manag. *257*, 1684–1694.

Chen, G., Hay, G.J., and Zhou, Y. (2010). Estimation of forest height, biomass and volume using support vector regression and segmentation from lidar transects and Quickbird imagery. In 2010 18th International Conference on Geoinformatics, pp. 1–4.

Chen, Q., Baldocchi, D., Gong, P., and Kelly, M. (2006). Isolating individual trees in a savanna woodland using small footprint lidar data. Photogramm. Eng. Remote Sens. *72*, 923–932.

Chen, Q., Vaglio Laurin, G., Battles, J.J., and Saah, D. (2012). Integration of airborne lidar and vegetation types derived from aerial photography for mapping aboveground live biomass. Remote Sens. Environ. *121*, 108–117.

Clark, D.B., and Kellner, J.R. (2012). Tropical forest biomass estimation and the fallacy of misplaced concreteness. J. Veg. Sci. *23*, 1191–1196.

Dalponte, M., Bruzzone, L., and Gianelle, D. (2008). Estimation of tree biomass volume in alpine forest areas using multireturn lidar data and support vector regression. p. 71090C – 71090C – 12.

Edson, C., and Wing, M.G. (2011). Airborne Light Detection and Ranging (LiDAR) for individual tree stem location, height, and biomass measurements. Remote Sens. *3*, 2494–2528.

Falkowski, M.J., Smith, A.M., Hudak, A.T., Gessler, P.E., Vierling, L.A., and Crookston, N.L. (2006). Automated estimation of individual conifer tree height and crown diameter via two-dimensional spatial wavelet analysis of lidar data. Can. J. Remote Sens. *32*, 153–161.

Garcıa-Gutiérreza, J., Martınez-Álvarezb, F., Troncosob, A., and Riquelmea, J.C. A comparison of machine learning regression techniques for LiDAR-derived estimation of forest variables.

Gibbs, H.K., Brown, S., Niles, J.O., and Foley, J.A. (2007). Monitoring and estimating tropical forest carbon stocks: making REDD a reality. Environ. Res. Lett. *2*, 045023.

Gleason, C.J., and Im, J. (2012). Forest biomass estimation from airborne LiDAR data using machine learning approaches. Remote Sens. Environ. *125*, 80–91.

Hall, S.A., Burke, I.C., Box, D.O., Kaufmann, M.R., and Stoker, J.M. (2005). Estimating stand structure using discrete-return lidar: an example from low density, fire prone ponderosa pine forests. For. Ecol. Manag. *208*, 189–209.

Heath, L.S., Hansen, M., Smith, J.E., Miles, P.D., and Smith, B.W. (2008). Investigation into calculating tree biomass and carbon in the FIADB using a biomass expansion factor approach. McWilliams WH Moisen GG Czaplewski RL Eds.

Hyyppa, J., Kelle, O., Lehikoinen, M., and Inkinen, M. (2001). A segmentation-based method to retrieve stem volume estimates from 3-D tree height models produced by laser scanners. Geosci. Remote Sens. IEEE Trans. On *39*, 969–975.

Jenkins, J.C., Chojnacky, D.C., Heath, L.S., and Birdsey, R.A. (2003). National-Scale Biomass Estimators for United States Tree Species. For. Sci. *49*, 12–35.

Koetz, B., Sun, G., Morsdorf, F., Ranson, K.J., Kneubühler, M., Itten, K., and Allgöwer, B. (2007). Fusion of imaging spectrometer and LIDAR data over combined radiative transfer models for forest canopy characterization. Remote Sens. Environ. *106*, 449–459.

Kwak, D.-A., Lee, W.-K., Lee, J.-H., Biging, G.S., and Gong, P. (2007). Detection of individual trees and estimation of tree height using LiDAR data. J. For. Res. *12*, 425–434.

Lefsky, M.A., Harding, D., Cohen, W.B., Parker, G., and Shugart, H.H. (1999). Surface Lidar Remote Sensing of Basal Area and Biomass in Deciduous Forests of Eastern Maryland, USA. Remote Sens. Environ. *67*, 83–98.

Lefsky, M.A., Turner, D.P., Guzy, M., and Cohen, W.B. (2005). Combining lidar estimates of aboveground biomass and Landsat estimates of stand age for spatially extensive validation of modeled forest productivity. Remote Sens. Environ. *95*, 549–558.

Lucas, R.M., Lee, A.C., and Bunting, P.J. (2008). Retrieving forest biomass through integration of CASI and LiDAR data. Int. J. Remote Sens. *29*, 1553–1577.

Mascaro, J., Detto, M., Asner, G.P., and Muller-Landau, H.C. (2011). Evaluating uncertainty in mapping forest carbon with airborne LiDAR. Remote Sens. Environ. *115*, 3770–3774.

McMahon, T. (1971). Size and shape in biology. Sci Amer *224*, 224.

Means, J.E., Acker, S.A., Harding, D.J., Blair, J.B., Lefsky, M.A., Cohen, W.B., Harmon, M.E., and McKee, W.A. (1999). Use of Large-Footprint Scanning Airborne Lidar To Estimate Forest Stand Characteristics in the Western Cascades of Oregon. Remote Sens. Environ. *67*, 298–308.

Myneni, R.B., Dong, J., Tucker, C.J., Kaufmann, R.K., Kauppi, P.E., Liski, J., Zhou, L., Alexeyev, V., and Hughes, M.K. (2001). A large carbon sink in the woody biomass of northern forests. Proc. Natl. Acad. Sci. *98*, 14784–14789.

Nelson, B.W., Mesquita, R., Pereira, J.L., De Souza, S.G.A., Batista, G.T., and Couto, L.B. (1999). Allometric regressions for improved estimate of secondary forest biomass in the central Amazon. For. Ecol. Manag. *117*, 149–167.

Niklas, K.J. (1995). Size-dependent Allometry of Tree Height, Diameter and Trunk-taper. Ann. Bot. *75*, 217–227.

O'Brien, S.T., Hubbell, S.P., Spiro, P., Condit, R., and Foster, R.B. (1995). Diameter, Height, Crown, and Age Relationship in Eight Neotropical Tree Species. Ecology *76*, 1926–1939.

Pacala, S.W., Hurtt, G.C., Baker, D., Peylin, P., Houghton, R.A., Birdsey, R.A., Heath, L., Sundquist, E.T., Stallard, R.F., Ciais, P., et al. (2001). Consistent Land- and Atmosphere-Based U.S. Carbon Sink Estimates. Science *292*, 2316–2320.

Pan, Y., Birdsey, R.A., Fang, J., Houghton, R., Kauppi, P.E., Kurz, W.A., Phillips, O.L., Shvidenko, A., Lewis, S.L., Canadell, J.G., et al. (2011). A Large and Persistent Carbon Sink in the World's Forests. Science *333*, 988–993.

Patenaude, G., Hill, R.., Milne, R., Gaveau, D.L.A., Briggs, B.B.J., and Dawson, T.P. (2004). Quantifying forest above ground carbon content using LiDAR remote sensing. Remote Sens. Environ. *93*, 368–380.

Swatantran, A., Dubayah, R., Roberts, D., Hofton, M., and Blair, J.B. (2011). Mapping biomass and stress in the Sierra Nevada using lidar and hyperspectral data fusion. Remote Sens. Environ. *115*, 2917–2930.

Ter-Mikaelian, M.T., and Korzukhin, M.D. (1997). Biomass equations for sixty-five North American tree species. For. Ecol. Manag. *97*, 1–24.

Zhao, F., Guo, Q., and Kelly, M. (2012). Allometric equation choice impacts lidar-based forest biomass estimates: A case study from the Sierra National Forest, CA. Agric. For. Meteorol. *165*, 64–72.

Zhou, X., and Hemstrom, M.A. (2010). Timber volume and aboveground live tree biomass estimations for landscape analyses in the Pacific Northwest.

Zianis, D., and Seura, S.M. (2005). Biomass and stem volume equations for tree species in Europe (Finnish Society of Forest Science, Finnish Forest Research Institute).

Zolkos, S.G., Goetz, S.J., and Dubayah, R. (2013). A meta-analysis of terrestrial aboveground biomass estimation using lidar remote sensing. Remote Sens. Environ. *128*, 289–298.